Characterizing Oxygen Local Environments in Paramagnetic Battery Materials via ^{17}O NMR and DFT Calculations

Ieuan D. Seymour,[†] Derek S. Middlemiss,[‡] David M. Halat,[†] Nicole M. Trease,[†] Andrew J. Pell,[†,§] and Clare P. Grey*,[†]

[†]Department of Chemistry, University of Cambridge, Cambridge CB2 1EW, United Kingdom
[‡]Department of Chemistry, University of Warwick, Coventry CV4 7AL, United Kingdom
[§]Department of Materials and Environmental Chemistry, Stockholm University, Stockholm SE-106 91, Sweden

S *Supporting Information*

ABSTRACT: Experimental techniques that probe the local environment around O in paramagnetic Li-ion cathode materials are essential in order to understand the complex phase transformations and O redox processes that can occur during electrochemical delithiation. While Li NMR is a well-established technique for studying the local environment of Li ions in paramagnetic battery materials, the use of ^{17}O NMR in the same materials has not yet been reported. In this work, we present a combined ^{17}O NMR and hybrid density functional theory study of the local O environments in Li_2MnO_3, a model compound for layered Li-ion batteries. After a simple ^{17}O enrichment procedure, we observed five resonances with large ^{17}O shifts ascribed to the Fermi contact interaction with directly bonded Mn^{4+} ions. The five peaks were separated into two groups with shifts at 1600 to 1950 ppm and 2100 to 2450 ppm, which, with the aid of first-principles calculations, were assigned to the ^{17}O shifts of environments similar to the 4i and 8j sites in pristine Li_2MnO_3, respectively. The multiple O environments in each region were ascribed to the presence of stacking faults within the Li_2MnO_3 structure. From the ratio of the intensities of the different ^{17}O environments, the percentage of stacking faults was found to be ca. 10%. The methodology for studying ^{17}O shifts in paramagnetic solids described in this work will be useful for studying the local environments of O in a range of technologically interesting transition metal oxides.

Lithium transition metal (TM) oxides with the layered $LiTMO_2$ structure continue to be the most promising cathode materials to replace $LiCoO_2$ in Li-ion batteries. Within the layered $LiTMO_2$ family of materials, $Li(Ni_{1−x−y}Co_xAl_y)O_2$ (NCA)[1,2] and $Li(Ni_{1−x−y}Mn_xCo_y)O_2$[3,4] (NMC) have reached commercialization, and other systems such as $(1 − x)Li_2MnO_3 \cdot xLiNi_{0.5}Mn_{0.5}O_2$ (Li−Mn rich)[5] are still generating significant research efforts, driven by the low cost and high theoretical capacity of these materials. In all of these systems, phase transformations involving the migration of TM ions have been found to occur, resulting in the formation of "spinel-like" (space group $Fd\bar{3}m$) or rock salt (space group $Fm\bar{3}m$) structures, particularly at the surface of electrochemically delithiated

particles.[6−8] Methods to prevent the phase transformations have been actively investigated, as it has been shown that they lead to irreversible capacity losses. The exact processes by which the phase transformations occur are not well understood, but in many cases the proposed mechanism depends sensitively on the nature of the O environment. In a number of layered systems, the phase transformation is accompanied by the loss of O_2 from the structure.[6,9] O can also play a beneficial role in $LiTMO_2$ materials by undergoing redox reactions that provide extra capacity beyond the TM redox. The mechanism by which reversible redox occurs on O has been studied using a number of different techniques. The formation of peroxo ($O_2^{2−}$) or superoxo ($O_2^−$) species has been proposed for 4d systems such as $Li_2Ru_{1−y}Sn_yO_3$,[10] whereas the formation of localized electron holes has been proposed in other systems, such as Li-rich NMC.[11,12] The ability to probe the local O environments in these systems is essential in order to gain a deeper understanding of the nature of the phase transformations and O redox.

$^{6/7}Li$ solid-state NMR spectroscopy has previously been shown to be a powerful technique for the study of local structure in paramagnetic battery materials.[13] However, despite the prevalence of O in these materials, the number of studies using ^{17}O NMR spectroscopy is significantly lower because of the low natural abundance of ^{17}O (0.037%) and the large quadrupole moment of the spin $I = ^5/_2$ nucleus.[14] A further complication in these paramagnetic systems is that the spin-bearing center is often directly bonded to O, resulting in large shifts and broad spectra. Static (and broad) ^{17}O solid-state NMR spectra of O ions adjacent to Mn^{4+} sites were obtained in $CaMnO_3$ manganite[15] by using frequency-stepped NMR spectroscopy. In a recent study, Kong et al.[16] used fast magic-angle spinning (MAS) at frequencies of 45−65 kHz to resolve ^{17}O resonances of O directly bonded to TM centers for a range of V^{3+}, Cu^{2+}, and Mn^{3+} complexes.

In this study, we demonstrate the first use of ^{17}O solid-state MAS NMR spectroscopy for a paramagnetic battery material, here Li_2MnO_3. To assign the large paramagnetic shifts, which are dominated by the Fermi contact interaction, and to characterize the broad spinning-sideband manifolds, which have contributions from the electron−nuclear dipolar and quad-

rupolar interactions, solid-state hybrid density functional theory (DFT) calculations were used, as in previous work.[17−19] Li_2MnO_3 was chosen as a model system for the layered $LiTMO_2$ systems, as it is the end member of the $(1 − x)Li_2MnO_3 \cdot xLiNi_{0.5}Mn_{0.5}O_2$ family of materials.

Li_2MnO_3 (Figure 1a) can be written in the layered notation as $Li[Li_{1/3}Mn_{2/3}]O_2$ and consists of layers of Li (Figure 1b) and
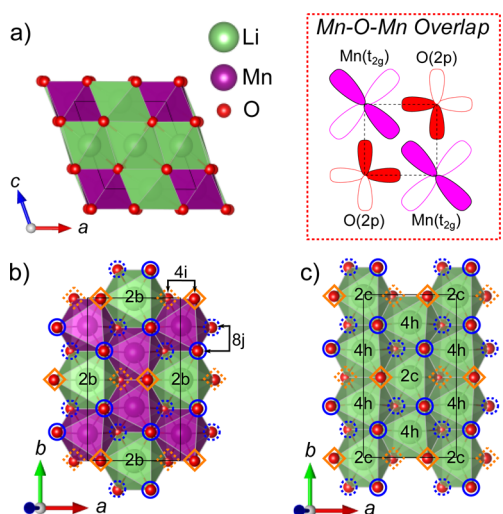

Figure 1. Schematic representations of (a) the unit cell of Li_2MnO_3 with space group $C2/m$, (b) the $Li_{1/3}Mn_{2/3}$ "honeycomb" (001) layer, and (c) the Li (002) layer. The 4i and 8j O sites are highlighted with orange diamonds and blue circles, respectively. The 2b, 2c, and 4h Li sites are labeled directly. The ∼90° Mn−O−Mn orbital overlap for the 4i and 8j sites is shown in the inset (red dashed box).

$Li_{1/3}Mn_{2/3}$ (Figure 1c) alternating along the c direction in an O close-packed lattice. The majority of studies suggest that Li_2MnO_3 adopts the $C2/m$ structure,[20] but depending on the synthesis temperature, significant structural defects involving stacking of the $Li_{1/3}Mn_{2/3}$ (honeycomb) planes along the c axis of the cell are known to occur.[21,22] In the work of Bréger et al.,[21] stacking sequences of $Li_{1/3}Mn_{2/3}$ layers, such as in the $P3_112$ structure (section S1 in the Supporting Information),

containing a threefold screw axis along the c axis, were considered to model the stacking faults in the $C2/m$ structure, leading to new Li and O local environments.

Li_2MnO_3 was synthesized by a conventional solid-state approach, as described in section S2. Because of the low natural abundance of ^{17}O, Li_2MnO_3 was ^{17}O-enriched using a simple procedure in which the as-synthesized material was heated in a $^{17}O_2$ environment after synthesis. Broad superstructure peaks were present at $2\theta = 20°$ to $35°$ in the powder X-ray diffraction patterns of both the as-synthesized and enriched materials (section S3), suggesting the presence of stacking faults of the $Li_{1/3}Mn_{2/3}$ layers, consistent with previous studies.[21,22] The 11.7 T and 60 kHz MAS ^{17}O NMR variable-offset cumulative spectroscopy (VOCS)[23] spectrum of the enriched Li_2MnO_3 material is shown in Figure 2a. Five individual subspectra were acquired at different offset frequencies and summed as shown in section S4. Two groups of resonances, region X (2100 to 2450 ppm) and region Y (1600 to 1950 ppm) containing five individual isotropic peaks in total were observed at 1721, 1859, 2211, 2231, and 2373 ppm (Figure 2b). The fitting procedure used to deconvolute the peaks was aided by the use of hybrid-DFT-computed parameters describing the quadrupolar and dipolar contributions to the line shape and is detailed in section S5. Spectra at 60 kHz MAS were taken at different magnetic field strengths (4.7 and 16.4 T) to confirm that the five peaks were due to multiple O environments rather than quadrupolar line-shape effects (section S6). While low magnetic fields (4.7 T here) are useful for reducing the magnitude of the electron−nuclear dipolar couplings, the resulting increase in the second-order quadrupolar broadening did not allow the different O sites in this structure to be resolved.

There are only two O positions in the perfectly ordered Li_2MnO_3 $C2/m$ structure, namely, the 4i and 8j sites, while at least five peaks, and thus five local environments, are observed in the ^{17}O NMR spectrum. The assignment of peak regions to particular environments was made with the aid of hybrid DFT calculations using the pristine $C2/m$ structure and a $P3_112$ structure containing different stackings of the $Li_{1/3}Mn_{2/3}$ layers along the c axis (a full description of the computational methodology is provided in in sections S7−S10). Previous studies have shown that the hyperfine shift depends strongly on
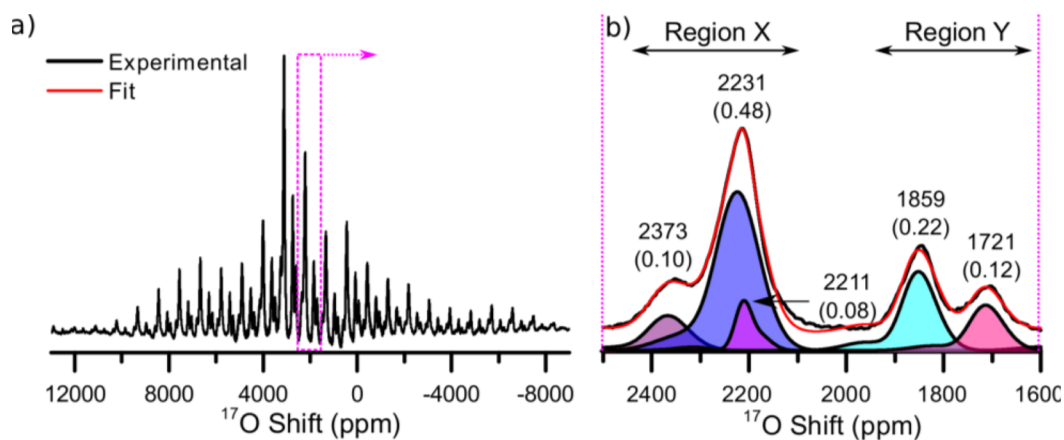
Figure 2. ^{17}O NMR VOCS spectrum of ^{17}O-enriched Li_2MnO_3 at 11.7 T and 60 kHz MAS showing (a) the spinning-sideband manifolds with isotropic resonances highlighted (magenta dashed box), and (b) an expanded view of the isotropic resonances showing the two regions of ^{17}O shifts, X (2100 to 2450 ppm) and Y (1600 to 1950 ppm). Also shown are the five individually deconvoluted peaks (shaded) with the resulting fit (red line). The unbracketed numbers above the resonances provide the ^{17}O shifts in ppm, and the bracketed numbers give the fractions of the different O environments in the total integral of the isotropic region.

the amount of Fock exchange incorporated into the hybrid functional, with 20% (HYB20) and 35% (HYB35) yielding reasonable upper and lower bounds of the shifts, respectively.[17] The shifts predicted for the two O sites in the $C2/m$ structure and three sites in the $P3_112$ structure are shown in Table 1. All

Table 1. DFT-Computed ^{17}O Hyperfine Shifts for O Sites in the $C2/m$ and $P3_112$ structures of Li$_2$MnO$_3$ at 340 K (Sample Temperature at 60 kHz MAS); The Values Calculated with the HYB20 and HYB35 Hybrid Functionals Are Shown

| structure	O site	^{17}O Shift (ppm)	
		HYB20	HYB35
$C2/m$	4i	2172	1327
	8j	2506	1529
$P3_112$	6c [1]	2060	1174
	6c [2]	2502	1524
	6c [3]	2613	1679

of the experimentally observed ^{17}O shifts fall within the HYB20 to HYB35 range. In the $C2/m$ structure, the 8j site is predicted to have a larger shift than the 4i site by 202 to 334 ppm. The shift difference can be understood by considering the variation in the local bonding around the ^{17}O site. Both O ions are directly bonded to two octahedral Mn^{4+} species through a π-type O(2p)−Mn(t$_{2g}$) interaction, forming an approximately 90° Mn−O−Mn pathway (Figure 1 inset). The mean Mn−O distances in the HYB20 structure are 1.910 and 1.899 Å for the 4i and 8j sites, respectively, consistent with a larger degree of overlap of Mn and O orbitals for the 8j site and thus a larger shift. The stacking of the Li$_{1/3}$Mn$_{2/3}$ layers also affects the ^{17}O shifts, as can be seen from the $P3_112$ structure. The $P3_112$ stacking leads to three distinct O sites (section S6) with Mn−O pathway contributions similar to those of the 4i and 8j sites. The small differences between the shifts of the groups of O sites in the pristine $C2/m$ and $P3_112$ structures are due to differences in additional bond pathways with Mn^{4+} ions beyond the first-nearest-neighbor environment.

The DFT results allow the peaks in Figure 2 to be rationalized. The shift difference of 372 ppm between the two most intense peaks in regions Y and X at 1859 and 2231 ppm matches well with the shift difference predicted for the $C2/m$ structure, which suggests that these can be assigned to the 4i and 8j sites, respectively. The ^{17}O shifts of the $P3_112$ structure indicate that different stacking sequences of the Li$_{1/3}$Mn$_{2/3}$ (honeycomb) planes in the c direction generate noticeably different O hyperfine shifts. The additional peaks at 1721, 2211, and 2373 ppm in Figure 2 are thus assigned to stacking faults of the Li$_{1/3}$Mn$_{2/3}$ layers. The O environments in the stacking faults constitute 30% of the total ^{17}O intensity. As shown in section S11, this distribution of O environments can be rationalized on the basis of a model in which a stacking fault of the ordered $C2/m$ structure occurs every 10 Li$_{1/3}$Mn$_{2/3}$ layers, i.e., with 10% stacking faults. This result is in excellent agreement with the study of Bréger et al.,[21] in which 10% stacking faults were predicted from DIFFAX simulations for a sample synthesized under similar conditions.

Finally, the dominant interaction leading to the broad spinning-sideband manifold observed in Figure 2a can be assessed from the first-principles calculations. The sizes of the electron−nuclear dipolar and quadrupole interactions for all O sites in both structures were calculated and are shown in

section S10. A comparison of the experimental spectrum with spectra simulated using the average computed electron−nuclear dipolar and quadrupolar parameters given in section S5 is shown in Figure 3. The main contribution to the spinning-
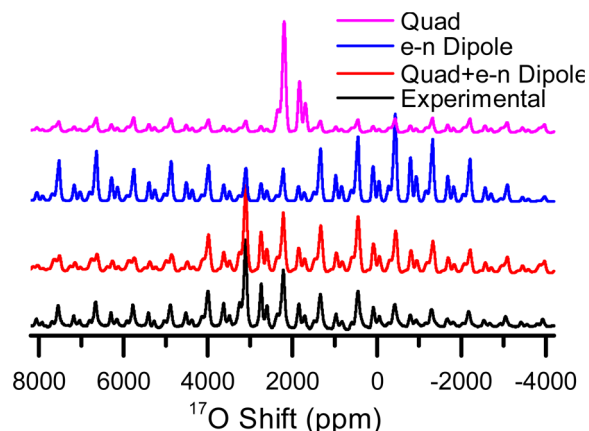
Figure 3. Comparison of the sideband manifolds of the experimental ^{17}O spectrum of Li$_2$MnO$_3$ (black) at 11.7 T with sideband manifolds calculated by considering various combinations of the contributions from the quadrupolar and electron−nuclear dipolar interactions as predicted from first-principles calculations. The dipolar and quadrupolar parameters correspond to those shown in section S5.

sideband manifold at 11.7 T in Figure 3 is the large shift anisotropy $\Delta\delta_D$ due to the large electron−nuclear dipolar coupling of approximately 10 000 ppm. However, good agreement with the experimental pattern emerges only when both the electron−nuclear dipolar coupling and the large quadrupolar coupling, C_q, of approximately 4.6 MHz are considered.

In summary, the ^{17}O NMR spectrum of Li$_2$MnO$_3$ was obtained following ^{17}O enrichment. Large ^{17}O shifts were observed, originating from a Fermi contact interaction with Mn^{4+} ions that are directly bonded to the O ions. Hybrid DFT calculations assigned the most intense isotropic resonances to the 4i and 8j sites in the $C2/m$ structure. The sensitivity of ^{17}O NMR spectroscopy to structural defects in the material was demonstrated by the observation of additional resonances associated with stacking faults within the structure. The nature of the broad spinning-sideband manifold could also be rationalized with hybrid DFT calculations, which revealed that both the electron−nuclear dipolar and quadrupole interactions are significant. The combined experimental and computational methodology outlined in this work is expected to be extremely useful for studying O local environments in a range of technologically relevant paramagnetic materials.

■ ASSOCIATED CONTENT

Ⓢ Supporting Information

The Supporting Information is available free of charge on the ACS Publications website at DOI: 10.1021/jacs.6b05747.

All experimental and computational details and the ^{17}O NMR fitting procedure (PDF)

■ AUTHOR INFORMATION

Corresponding Author

*cpg27@cam.ac.uk

Notes

The authors declare no competing financial interest.

■ REFERENCES

(1) Madhavi, S.; Subba Rao, G. V.; Chowdari, B. V. R.; Li, S. F. Y. *J. Power Sources* **2001**, *93*, 156.

(2) Weaving, J. S.; Coowar, F.; Teagle, D. A.; Cullen, J.; Dass, V.; Bindin, P.; Green, R.; Macklin, W. J. *J. Power Sources* **2001**, *97-98*, 733.

(3) Lu, Z.; MacNeil, D. D.; Dahn, J. R. *Electrochem. Solid-State Lett.* **2001**, *4*, A200.

(4) Yabuuchi, N.; Ohzuku, T. *J. Power Sources* **2003**, *119-121*, 171.

(5) Lu, Z.; MacNeil, D. D.; Dahn, J. R. *Electrochem. Solid-State Lett.* **2001**, *4*, A191.

(6) Hwang, S.; Chang, W.; Kim, S. M.; Su, D.; Kim, D. H.; Lee, J. Y.; Chung, K. Y.; Stach, E. A. *Chem. Mater.* **2014**, *26*, 1084.

(7) Lin, F.; Markus, I. M.; Nordlund, D.; Weng, T.-C.; Asta, M. D.; Xin, H. L.; Doeff, M. M. *Nat. Commun.* **2014**, *5*, 3529.

(8) Xu, B.; Fell, C. R.; Chi, M.; Meng, Y. S. *Energy Environ. Sci.* **2011**, *4*, 2223.

(9) Armstrong, A. R.; Holzapfel, M.; Novák, P.; Johnson, C. S.; Kang, S.-H.; Thackeray, M. M.; Bruce, P. G. *J. Am. Chem. Soc.* **2006**, *128*, 8694.

(10) Sathiya, M.; Rousse, G.; Ramesha, K.; Laisa, C. P.; Vezin, H.; Sougrati, M. T.; Doublet, M.-L.; Foix, D.; Gonbeau, D.; Walker, W.; Prakash, A. S.; Ben Hassine, M.; Dupont, L.; Tarascon, J.-M. *Nat. Mater.* **2013**, *12*, 827.

(11) Luo, K.; Roberts, M. R.; Hao, R.; Guerrini, N.; Pickup, D. M.; Liu, Y.-S.; Edström, K.; Guo, J.; Chadwick, A. V.; Duda, L. C.; Bruce, P. G. *Nat. Chem.* **2016**, *8*, 684.

(12) Seo, D.-H.; Lee, J.; Urban, A.; Malik, R.; Kang, S.; Ceder, G. *Nat. Chem.* **2016**, *8*, 692.

(13) Grey, C. P.; Dupré, N. *Chem. Rev.* **2004**, *104*, 4493.

(14) Ashbrook, S. E.; Smith, M. E. *Chem. Soc. Rev.* **2006**, *35*, 718.

(15) Verkhovskii, S.; Trokiner, A.; Gerashenko, A.; Yakubovskii, A.; Medvedeva, N.; Litvinova, Z.; Mikhalev, K.; Buzlukov, A. *Phys. Rev. B: Condens. Matter Mater. Phys.* **2010**, *81*, 144415.

(16) Kong, X.; Terskikh, V. V.; Khade, R. L.; Yang, L.; Rorick, A.; Zhang, Y.; He, P.; Huang, Y.; Wu, G. *Angew. Chem., Int. Ed.* **2015**, *54*, 4753.

(17) Kim, J.; Middlemiss, D. S.; Chernova, N. A.; Zhu, B. Y. X.; Masquelier, C.; Grey, C. P. *J. Am. Chem. Soc.* **2010**, *132*, 16825.

(18) Middlemiss, D. S.; Ilott, A. J.; Clément, R. J.; Strobridge, F. C.; Grey, C. P. *Chem. Mater.* **2013**, *25*, 1723.

(19) Clément, R. J.; Pell, A. J.; Middlemiss, D. S.; Strobridge, F. C.; Miller, J. K.; Whittingham, M. S.; Emsley, L.; Grey, C. P.; Pintacuda, G. *J. Am. Chem. Soc.* **2012**, *134*, 17178.

(20) Strobel, P.; Lambert-Andron, B. *J. Solid State Chem.* **1988**, *75*, 90.

(21) Bréger, J.; Jiang, M.; Dupré, N.; Meng, Y. S.; Shao-Horn, Y.; Ceder, G.; Grey, C. P. *J. Solid State Chem.* **2005**, *178*, 2575.

(22) Boulineau, A.; Croguennec, L.; Delmas, C.; Weill, F. *Chem. Mater.* **2009**, *21*, 4216.

(23) Pell, A. J.; Clément, R. J.; Grey, C. P.; Emsley, L.; Pintacuda, G. *J. Chem. Phys.* **2013**, *138*, 114201.